Polarization Descattering Imaging of Underwater Complex Targets Based on Mueller Matrix Decomposition

Yuanzhi Zhao, Wenjun He, Hang Ren, Yuhui Zhang, and Yuegang Fu, *Member, IEEE*

***Abstract*—The traditional polarization imaging techniques cannot obtain the polarization characteristics with global variation, and the reconstruction of the target with different optical properties concurrently is seriously distorted. In this work, we overcome the aforementioned shortcomings by using the polar decomposition method to estimate the Mueller matrix of the target in the full field of view. Simultaneously, the illumination light with globally varying polarization state is calculated to suppress the noise caused by computational imaging. The descattering imaging experiments through turbid water indicate that the images recovered by our method present the similarity to the targets without scattering, and the noise is suppressed to some extent. Further, we prove the superiority of the proposed method by comparing with other polarization underwater imaging strategies.**

***Index Terms*—Polarimetric imaging, mueller matrix, scattering measurements, turbid media.**

I. Introduction

UNDERWATER imaging technology has important applications in marine resource exploration, underwater rescue, and other fields [1], [2], [3]. However, the light can be absorbed and scattered (both forward and backward) by the particles in natural water. Therein forward scattered light is reflected by objects and then is diffused back to the detector, which generally blurs the images. Backscattered light is reflected by particles back to the detector before reaching the object, and the main negative effect is to degrade the contrast of immerged objects because of the veil that superimposes on the image [4]. All of them can lead to the serious reduction in image quality [5]. Therefore, there is an urgent need to seek for an effective way for recovering the underwater image [6].

To solve this problem, many imaging methods have been proposed [7], [8], [9], [10], [11]. Among them, polarization imaging, which uses the difference of the polarization characteristics of the target signal and scattered light to remove the scattering effect, has received extensive attention [12], [13], [14], [15]. In the existing polarization descattering model, it is especially important to estimate the degree of polarization (DoP) of target light and backscattered light accurately. However, most of the previous studies estimated the DoP of target light as a constant value because the full field of view (FOV) variation cannot be obtained [16], [17], [18]. In addition, according to the theory proposed by Treibitz et al. [19], it is beneficial for reducing noise and achieving a better descattering imaging effect by increasing the difference between the DoP of target light and backscattered light, but so far it has been rarely focused. In fact, it is almost impossible to maximize the difference between the two DoP unless the polarization properties of the target and scattering medium are known to a large extent.

In this paper, we demonstrate a method to obtain the polarization characteristics of complex targets based on Mueller matrix polar decomposition for underwater descattering imaging. The depolarization vector of the least related target and scattering medium is estimated by the mutual information minimization method, and the global varying Mueller matrix of the target is further decoupled. Then the polarization state of incident light which maximizes the difference of DoP between target light and backscattered light is calculated to minimize the noise of descattering imaging. The experimental results show that the method can achieve the imaging and recognition of complex objects with a low noise in turbid water. In addition, the experimental results on targets consisting of different materials and water turbidity prove that our method is available and effective.

II. Theory and Method

A. Mathematic Model of the Underwater Polarization Imaging and Effectiveness Under Noise

According to the image formation theory, an underwater image is the incoherent sum of the target signal and backscattered light [19], [20], [21],

$$I(x, y) = T(x, y) + B(x, y), \tag{1}$$

where $T(x, y)$ indicates target signal and $B(x, y)$ indicates backscattered light. However, owing to absorption and scattering by particles in water, the target irradiance $T(x, y)$ will be attenuated. In general, when using linear polarized light for illumination, both $T(x, y)$ and $B(x, y)$ are partially linear polarized. Based on polarization imaging technology, placing

Manuscript received 8 June 2022; revised 8 August 2022; accepted 4 September 2022. Date of publication 7 September 2022; date of current version 21 September 2022. This work was supported by the National Natural Science Foundation of China (NSFC) under Grant 61805025. *(Corresponding author: Yuegang Fu.)*

Yuanzhi Zhao, Wenjun He, Hang Ren, and Yuhui Zhang are with the Department of Optical Engineering, Changchun University of Science and Technology, Changchun 130012, China (e-mail: 1059228119@qq.com; hewenjun@cust.edu.cn; renh@cust.edu.cn; 2022800005@cust.edu.cn).

Yuegang Fu is with the Changchun University of Science and Technology, Changchun 130012, China (e-mail: fuyg@cust.edu.cn).

Digital Object Identifier 10.1109/JPHOT.2022.3204832

an analyzer in front of the camera and a pair of the images of the brightest and darkest scene generated when rotating the analyzer are represented by $I_{\max}(x, y)$ and $I_{\min}(x, y)$ respectively. Thus, (2) can be obtained from (1),

$$\begin{cases} I_{\max}(x,y) = T_{\max}(x,y) + B_{\max}(x,y) \\ I_{\min}(x,y) = T_{\min}(x,y) + B_{\min}(x,y) \end{cases}, \tag{2}$$

where $T_{\max}(x, y)$ and $B_{\max}(x, y)$ indicate target and backscattered light in $I_{\max}(x, y)$; $T_{\min}(x, y)$ and $B_{\min}(x, y)$ indicate target and backscattered light in $I_{\min}(x, y)$. In addition, the degree of linear polarization (DoLP) of target light and backscattered light $P_{\mathrm{obj}}(x, y)$ and $P_{\mathrm{sca}}(x, y)$ can be expressed as

$$\begin{cases} P_{obj}(x,y) = \frac{T_{\max}(x,y) - T_{\min}(x,y)}{T_{\max}(x,y) + T_{\min}(x,y)} \\ P_{sca}(x,y) = \frac{B_{\max}(x,y) - B_{\min}(x,y)}{B_{\max}(x,y) + B_{\min}(x,y)} \end{cases}. \tag{3}$$

Combining (1)–(3), $T(x, y)$ and $B(x, y)$ can be expressed as

$$\begin{cases} T(x,y) = \frac{[I_{\min}(x,y)(1+P_{sca}(x,y)) - I_{\max}(x,y)(1-P_{sca}(x,y))]}{P_{sca}(x,y) - P_{obj}(x,y)} \\ B(x,y) = \frac{[I_{\max}(x,y)(1-P_{obj}(x,y)) - I_{\min}(x,y)(1+P_{obj}(x,y))]}{P_{sca}(x,y) - P_{obj}(x,y)} \end{cases}. \tag{4}$$

As can be seen from (4), when the polarization characteristic of the target is almost unchanged in the FOV, a single value P_{obj} can be used to replace $P_{\mathrm{obj}}(x, y)$ to realize the recovery of scattering images relatively easily. However, there will be great distortion in the case of complex target scattering.

Next, we consider the noise introduced during the descattering process. $I_{\max}(x, y)$ and $I_{\min}(x, y)$ are supposed to be statistically independent, the noise variances in $T(x, y)$ and $B(x, y)$ are

$$\begin{cases} \sigma_T^2 = \left(\frac{1+P_{sca}(x,y)}{P_{obj}(x,y) - P_{sca}(x,y)}\right)^2 \sigma^2_{I_{\min}(x,y)} \\ \qquad + \left(\frac{1-P_{sca}(x,y)}{P_{obj}(x,y) - P_{sca}(x,y)}\right)^2 \sigma^2_{I_{\max}(x,y)} \\ \sigma_B^2 = \left(\frac{1+P_{obj}(x,y)}{P_{obj}(x,y) - P_{sca}(x,y)}\right)^2 \sigma^2_{I_{\min}(x,y)} \\ \qquad + \left(\frac{1-P_{obj}(x,y)}{P_{obj}(x,y) - P_{sca}(x,y)}\right)^2 \sigma^2_{I_{\max}(x,y)} \end{cases}, \tag{5}$$

where $\sigma^2_{I_{\max}(x,y)}$ and $\sigma^2_{I_{\min}(x,y)}$ represent the noise in $I_{\max}(x, y)$ and $I_{\min}(x, y)$ [19]. Obviously, increasing the difference between $P_{obj}(x, y)$ and $P_{sca}(x, y)$ is beneficial to reducing the noise caused by computational imaging. However, it is impossible to maximize $|P_{obj}(x, y) - P_{sca}(x, y)|$ by changing the polarization state of the incident light without knowing the polarization characteristics of the target. In Section II-B and C, we will clarify the method to obtain the polarization characteristics of global varying targets based on Mueller matrix polar decomposition, and obtain the difference maximization $P_{obj}(x, y)$ and $P_{sca}(x, y)$ accordingly.

B. Mueller Matrix Polar Decomposition and Depolarization Vector

Combined with Muller matrix polar decomposition [22], the normalized Mueller matrix can be expressed as:

$$\mathbf{M} = M_{11} \begin{pmatrix} 1 & m_{12} & m_{13} & m_{14} \\ m_{21} & m_{22} & m_{23} & m_{24} \\ m_{31} & m_{32} & m_{33} & m_{34} \\ m_{41} & m_{42} & m_{43} & m_{44} \end{pmatrix} = \mathbf{M}_{\Delta} \cdot \mathbf{M}_R \cdot \mathbf{M}_D, \tag{6}$$

including

$$m_{ij} = \frac{M_{ij}}{M_{11}},\ i, j = 1, 2, 3, 4\,, \tag{7}$$

where $\mathbf{M}_{\Delta}$, $\mathbf{M}_R$, and $\mathbf{M}_D$ represent the sub-matrices of the medium: depolarization, phase retardance and diattenuation respectively. A large number of previous underwater transmission studies have shown that when the incident light contains no circularly polarized component, there is almost no circularly polarized component in the scattered light. Therefore, circular polarization is not involved in our study, Mueller matrix and Stokes vector are correspondingly changed to third order.

Next, the depolarization matrix $\mathbf{M}_{\Delta}$ can be expressed as:

$$\mathbf{M}_{\Delta} = \begin{bmatrix} 1 & \vec{0}^T \\ \vec{P}_{\Delta} & \mathbf{m}_{\Delta} \end{bmatrix}, \mathbf{m}_{\Delta} = (\mathbf{m}_{\Delta})^T\,, \tag{8}$$

in which $\vec{P}_{\Delta}$ denotes the polarizance vector of depolarizer. $\mathbf{m}_{\Delta}$ is a 2×2 symmetric matrix whose eigenvalues characterize the linear depolarization properties. Therefore, the depolarizing vector .$\vec{\Delta}$. can be constructed,

$$\vec{\Delta} = (\lambda_1, \lambda_2)^T\,, \tag{9}$$

in which λ_1 and λ_2 are the eigenvalues of $\mathbf{m}_{\Delta}$.

C. Imaging Algorithm and Principles

The light received by the camera in scattering imaging can be regarded as the incoherent superposition of target light, backscattered light and forward scattered light [23]. It can be expressed by Mueller matrix and Stokes vector as

$$\begin{aligned} \vec{S}_{out} = \mathbf{M}_{total} \cdot \vec{S}_{in} = (\alpha \cdot \mathbf{M}_{obj}(x,y) + \beta \cdot \boldsymbol{M}_{sca}(x,y) \\ + \gamma \cdot \mathbf{M}_{obj}(x,y) \cdot \mathbf{M}_{sca}(x,y)) \cdot \vec{S}_{in}\,, \end{aligned} \tag{10}$$

where $\vec{S}_{out}$ and $\vec{S}_{in}$ represent the Stokes vector of incident and scattered light, $\mathbf{M}_{\mathrm{obj}}(x, y)$, $\mathbf{M}_{\mathrm{sca}}(x, y)$ and $\mathbf{M}_{\mathrm{total}}(x, y)$ indicate the Mueller matrix of targets, scattering medium and the total received by the camera respectively. α, β and γ are the weight coefficients. Because of the absorption of water,

$$\alpha + \beta + \gamma < 1\,, \tag{11}$$

with the constraint $\alpha, \beta, \gamma > 0$. In addition, Mueller matrix elements are not sensitive to targets or uneven illumination [24]. Therefore, for underwater strongly scattering imaging, Mueller matrix without target region can be selected and $\mathbf{M}_{\mathrm{sca}}$ of full FOV can be taken as average by pixels.

Thus, there are 12 unknowns in (8) for a single pixel (3×3 $\mathbf{M}_{\mathrm{obj}}$ and α, β, γ), but only 9 equations can be obtained through

the double-rotating polarizer method which is described in detail in Section III (because of the redundant Stokes vector element S_0). Therefore, without taking any additional images, taking (11) as the constraint condition and based on mutual information (MI) minimization method, the $\mathbf{M}_{\mathrm{obj}}$ corresponding to the set of depolarization vectors $(\vec{\Delta}obj, \vec{\Delta}sca)$ with the least correlation obtained from the search is estimated to be the $\mathbf{M}_{\mathrm{obj}}$ of the pixel. *MI* can be obtained by (12) [25],

$$\overline{MI}(\vec{\Delta}_{obj}, \vec{\Delta}_{sca}) = \sum_{i=1}^{2}\sum_{j=1}^{2} p_{\lambda obj,\lambda sca}(\lambda_i^{obj}, \lambda_j^{sca}) \log \frac{p_{\lambda obj,\lambda sca}(\lambda_i^{obj}, \lambda_j^{sca})}{p_{\lambda obj}(\lambda_i^{obj}) \cdot p_{\lambda sca}(\lambda_j^{sca})}, \tag{12}$$

where $p_{\lambda obj,\lambda sca}(\lambda_i^{obj}, \lambda_j^{sca})$ is the joint probability distribution function of elements in $\vec{\Delta}_{obj}$ and $\vec{\Delta}_{sca}$. The marginal distribution functions of $\vec{\Delta}_{obj}$ and $\vec{\Delta}_{sca}$ are defined as $p_{\lambda obj}(\lambda_i^{obj})$ and $p_{\lambda sca}(\lambda_j^{sca})$, respectively. A wrong estimation of $\mathbf{M}_{\mathrm{obj}}(x, y)$ can increase the crosstalk between $\vec{\Delta}_{obj}$ and $\vec{\Delta}_{sca}$, and *MI* can quantify it.

After $\mathbf{M}_{\mathrm{obj}}(x, y)$ and $\mathbf{M}_{\mathrm{sca}}$ are obtained, $\vec{S}_{in}$ with minimal imaging noise can be searched and found. As circular polarization is not considered, the constraint conditions and the method for calculating $P_{obj}(x, y)$ and $P_{sca}(x, y)$ are shown in (13) and (14) respectively,

$$\vec{S}_{in} = (S_0, S_1, S_2)^T, \tag{13}$$

$$P_{obj,sca}(x, y) = \frac{\sqrt{S_1^2 + S_2^2}}{S_0}, \tag{14}$$

there are $S_0 \equiv 1 \geq \sqrt{S_1^2 + S_2^2}$ and $-1 \leq (S_1, S_2) \leq 1$. On the basis of the noise theory in Section II-A, $\vec{S}_{in}$ which minimizes $|P_{obj}(x, y)\text{-}P_{sca}(x, y)|$ is taken as the Stokes vector of the incident light and the global varying $\vec{S}_{in}(x, y)$ is calculated according to the pixels in turn. Because S_0 represents the total light intensity, $I_{max}(x, y)$ and $I_{min}(x, y)$ are expressed as (15). Finally, the recovered image $T(x, y)$ can be obtained by (4). The basic flow of our algorithm is shown in Fig. 1.

$$\begin{cases} I_{\max}(x, y) = \frac{S_{out}^0(x,y) + \sqrt{(S_{out}^1(x,y))^2 + (S_{out}^2(x,y))^2}}{2} \\ I_{\min}(x, y) = \frac{S_{out}^0(x,y) - \sqrt{(S_{out}^1(x,y))^2 + (S_{out}^2(x,y))^2}}{2} \end{cases}. \tag{15}$$

III. Experiment

We perform a group of underwater imaging experiments and the experimental setup is shown in Fig. 2. The LED light with a wavelength of 621±10nm emitted from the light source is modulated by collimator and polarizer to be parallel linearly polarized light to illuminate the target, and imaged by a monochrome camera (C13440-20CU from HAMAMATSU) through the analyzer. We use a transparent tank filled with clear water, and the rear wall and bottom of the tank are covered with absorbent material to reduce interferences.

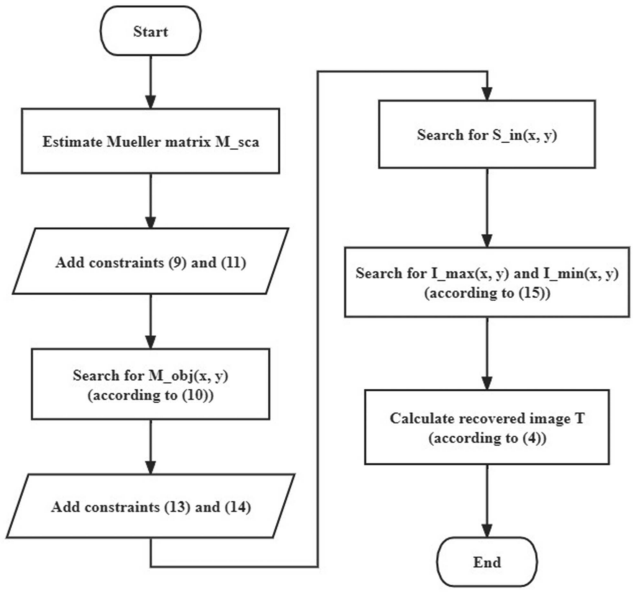

Fig. 1. The block diagram of our algorithm.

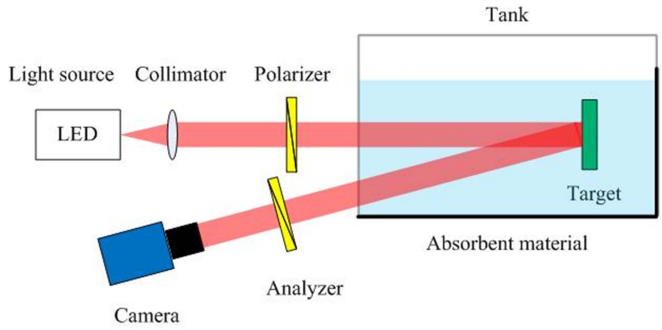

Fig. 2. Experimental setup for underwater imaging.

Next, we blend the water with skimmed milk so as to make it turbid, and place the target 70cm away from the front wall of the tank. The measured scattering coefficient of the medium $c = 1.15$. Then the Mueller matrix of FOV is obtained by the double-rotating polarizer method: by transforming the polarizer and analyzer into four polarization states of horizontal polarized (H), vertical polarized (V), 45° polarized (M) and 135° polarized (P) respectively. Then, 16 images are needed to obtain the Muller matrix $\mathbf{M}_{\mathrm{total}}$: (16) shown at the bottom of the next page.

Finally, the algorithm mentioned in Section II-C is used to obtain the descattering image.

IV. Results and Discussion

The first imaging target we choose is a coin placed on stone, and the intensity image with and without turbid water is shown in Fig. 3. Here, Peak signal-to-noise ratio (PSNR) and Structural Similarity (SSIM) are introduced as the objective image quality evaluation parameters [26], [27]. The larger the PSNR and SSIM, the more similar the two images are. By comparison with Fig. 3(a), it can be seen that the image degrades seriously

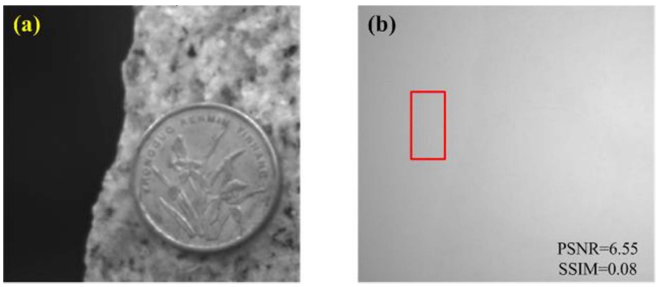

Fig. 3. Coin and stone. (a) Intensity image taken directly. (b) Intensity image in turbid water, The red box is the selected area without target.

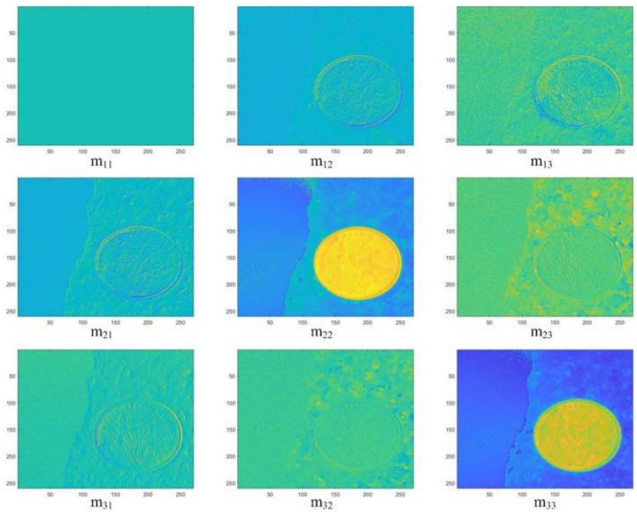

Fig. 4. The estimated normalized Mueller matrix image of the target.

after being scattered by turbid water. Firstly, we use the method mentioned in Section III to obtain the Mueller matrix $\mathbf{M}_{\text{total}}(x, y)$, and then estimate the Mueller matrix of the target $\mathbf{M}_{\text{obj}}(x, y)$ as shown in Fig. 4. It can be seen that our algorithm can suppress the scattered light and estimate $\mathbf{M}_{\text{obj}}(x, y)$ effectively. However, due to the error amplification caused by computational imaging, some elements of $\mathbf{M}_{\text{obj}}(x, y)$ have obvious noises.

Next, we estimate the polarization state of the light most suitable for descattering imaging theoretically, and the relevant parameters obtained are shown in Fig. 5. Although it can be seen that the polarization state may not be related to the target material or viewing angle, the DoLP of almost full FOV is close to 1 (yellow pixel area). It is worth mentioning that we guessed that in some situations, partially polarized light might be more beneficial to desscattering. However, the experimental results show that this hypothesis may not be tenable under the model presented in this paper.

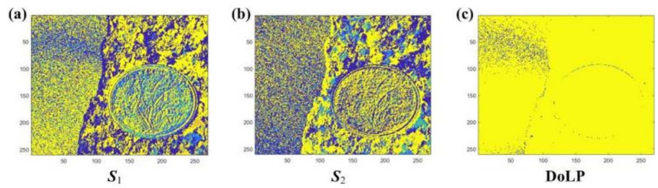

Fig. 5. Parameters of the estimated global varying incident light. (a) S_1. (b) S_2. (c) DoLP.

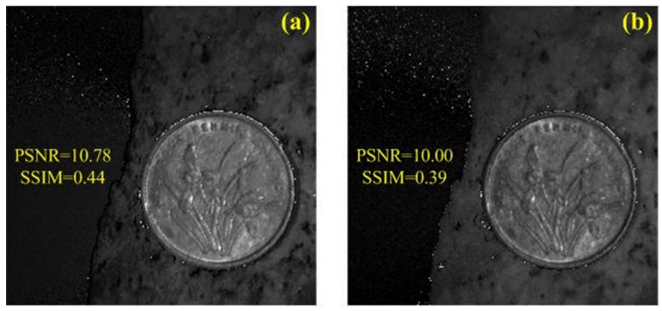

Fig. 6. Coin and stone. (a) Recovered image T by our method. (b) Descattering image obtained by using globally fixed polarized light.

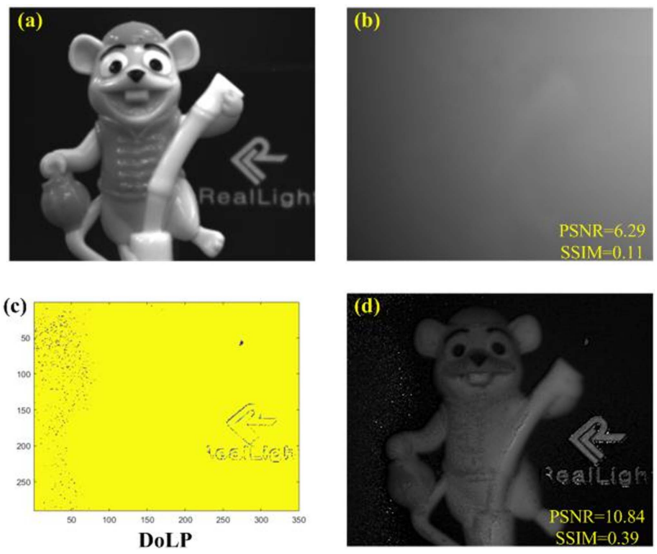

Fig. 7. Mouse and steel. (a) Intensity image taken directly. (b) Intensity image in turbid water. (c) DoLP of the estimated global varying incident light. (d) Recovered image T by our method.

The obtained descattering image T is shown as Fig. 6(a). It can be seen that compared with the intensity image taken directly in Fig. 3(b), the contrast of the recovered image is significantly improved and the identifiable details are richer. Moreover, PSNR and SSIM are significantly improved, indicating that the restored

$$\mathbf{M}_{total} = \frac{1}{2}\begin{pmatrix} HH+HV+VH+VV & HH+HV-VH-VV & PH+PV-MP-MM \\ HH-HV+VH-VV & HH-HV-VH+VV & PH-PV-MH+MV \\ HP-HM+VP-VM & HP-HM-VP+VM & PP-PM-MP+MM \end{pmatrix} \cdot \tag{16}$$

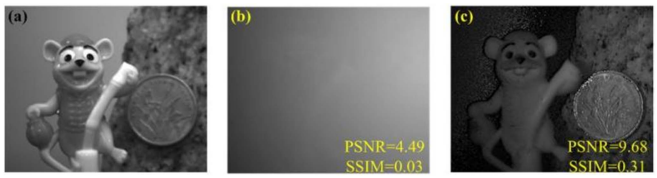

Fig. 8. Mouse, coin and stone. (a) Intensity image taken directly. (b) Intensity image in turbid water. (c) Recovered image T by our method.

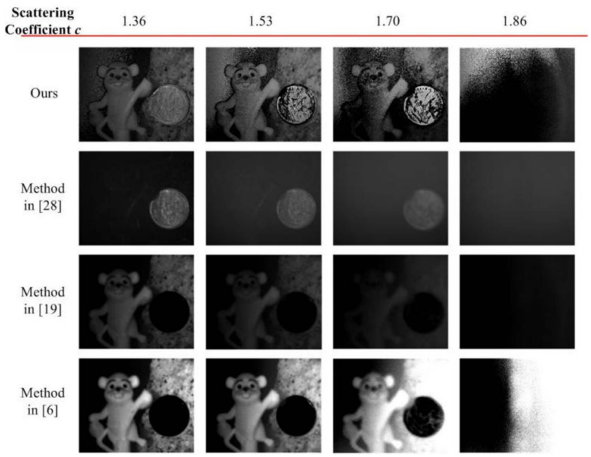

Fig. 9. Imaging comparison between our method and the others in different water turbidity.

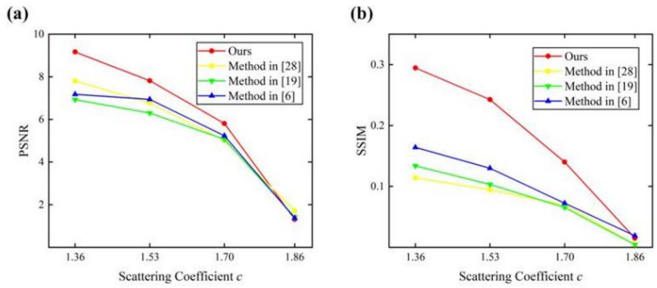

Fig. 10. Comparison of the parameters in different water turbidity. (a) PSNR. (b) SSIM.

image is closer to the clear image without scattering, and preliminary proves the effectiveness of our method. In addition, we also focus on the descattering with global fixed polarization illumination (e.g., $\vec{S}_{in} = (1, 1, 0, 0)^T$), and the result is shown as Fig. 6(b). It can be seen that compared with Fig. 6(a), the noise in Fig. 6(b) is stronger, the scene is slightly dark, PSNR and SSIM are also lower. Such result indicates that setting the polarized illumination as a global variable can suppress noise to a certain extent and improve the descattering effect.

Then, we replace the target with a plastic mouse and a piece of painted steel, the results obtained are shown in Fig. 7. It can be seen in Fig. 7(d) that the descattering imaging of our method is still effective, and Fig. 7(c) confirms the previous point ulteriorly. Moreover, the noise at the character edge is likely caused by the non-uniformity of the polarizer surface.

Furthermore, to investigate the universality of our method, we put the mouse, coin and stone in the same FOV to form a more complex target consisting of three materials, and the results are shown in Fig. 8. It can be seen that although the noise in the background area of the recovered image (Fig. 8(c)) has increased compared with that before, our method still shows descattering performance and certain robustness in general. It also indicates that the method can be combined with other image denoising algorithms for further optimization.

Finally, we investigate the effect of scattering intensity on our method by increasing the water turbidity and compare with other polarization descattering imaging methods, the results are shown in Figs. 9 and 10 [28]. Although it can be seen that the scope of application of our method is roughly the same as other methods, our method still possess prominent superiorities, which are mainly reflected in the simultaneous recovery of complex targets with widely varying polarization properties, both PSNR and SSIM are significantly higher. The method in [28] is more suitable for recovering the target with strong polarization maintaining characteristics, while the method in [19] is just the opposite. The P_{sca} estimated by [6] is close to the average of the DoLP of targets and the overall effect is better than [19]. Despite its high contrast, it is still not suitable for complex targets. In addition, due to the serious noise amplification caused by computational imaging in the strong scattering environment and PSNR is directly related to the noise, the PSNR improvement of our method seems to be lower than expected. It also shows that our method still has great room for improvement.

V. Conclusion

In conclusion, we combine Mueller matrix polar decomposition with underwater polarization imaging model, and propose a descattering imaging method suitable for the complex target and strongly scattering environment. The depolarization vector $\vec{\Delta}$ derived from Mueller matrix is constructed, then global varying Muller matrix of the target $\mathbf{M}_{\mathrm{obj}}(x, y)$ and incident light $\vec{S}_{in}(x, y)$ are scanned and calculated successively. Finally, the descattering imaging with noise reduction is achieved. The experimental results indicate that our method can effectively reconstruct the target with complex polarization characteristics in the same FOV and reduce the noise. Next, the robustness of the method is proved by the experimental results of increasing water turbidity. In addition, we present our method's benefits in comparison to other underwater polarization imaging methodologies. Our strategy can be applied to various areas including marine ranching and underwater construction, which can also provide some inspirations and guidance for further research.

Acknowledgment

F. A. Author would like to thank Xueming Xiao for helpful discussion. The authors would like to thank the Changchun University of Science and Technology (CUST) and Friedrich-Schiller-Universität Jena (FSU) Joint International Research Laboratory of Physical optics for the critical support and infrastructure provided for this work.

REFERENCES

[1] G. N. Bailey and N. C. Flemming, "Archaeology of the continental shelf: Marine resources, submerged landscapes and underwater archaeology," *Quaternary Sci. Rev.*, vol. 27, pp. 2153–2165, 2008, doi: 10.1016/j.quascirev.2008.08.012.

[2] D. M. Kocak, F. R. Dalgleish, F. M. Caimi, and Y. Y. Schechner, "A focus on recent developments and trends in underwater imaging," *Mar. Technol. Soc. J.*, vol. 42, pp. 52–67, 2008, doi: 10.4031/002533208786861209.

[3] L. B. Wolff, "Polarization vision: A new sensory approach to image understanding," *Image Vis. Comput.*, vol. 15, pp. 81–93, 1997, doi: 10.1016/S0262-8856(96)01123-7.

[4] M. Dubreuil et al., "Exploring underwater target detection by imaging polarimetry and correlation techniques," *Appl. Opt.*, vol. 52, no. 5, pp. 997–1005, 2013, doi: 10.1364/AO.52.000997.

[5] H. Hu, L. Zhao, B. Huang, X. Li, H. Wang, and T. Liu, "Enhancing visibility of polarimetric underwater image by transmittance correction," *IEEE Photon. J.*, vol. 9, no. 3, Jun. 2017 Art. no. 6802310, doi: 10.1109/JPHOT.2017.2698000.

[6] Y. Zhao et al., "Polarization descattering imaging through turbid water without prior knowledge," *Opt. Laser Eng.*, vol. 148, 2022, Art. no. 106777, doi: 10.1016/j.optlaseng.2021.106777.

[7] R. Schettini and S. Corchs, "Underwater image processing: State of the art of restoration and image enhancement methods," *EURASIP J. Adv. Signal Process.*, vol. 2010, pp. 1–14, Dec. 2010, doi: 10.1155/2010/746052.

[8] K. He, J. Sun, and X. Tang, "Single image haze removal using dark channel prior," *IEEE Trans. Pattern Anal. Mach. Intell.*, vol. 33, no. 12, pp. 2341–2353, Dec. 2011, doi: 10.1109/TPAMI.2010.168.

[9] F. R. Dalgleish, F. M. Caimi, A. K. Vuorenkoski, W. B. Britton, and B. Ramos, "Experiments in bistatic laser line scan (LLS) underwater imaging," in *Proc. Oceans*, 2009, pp. 1–9.

[10] L. Mullen, A. Laux, and B. Cochenour, "Propagation of modulated light in water: Implications for imaging and communications systems," *Appl. Opt.*, vol. 48, pp. 2607–2612, 2009, doi: 10.1364/AO.48.002607.

[11] H. Hu et al., "Polarimetric underwater image recovery via deep learning," *Opt. Laser Eng.*, vol. 133, 2020, Art. no. 106152, doi: 10.1016/j.optlaseng.2020.106152.

[12] Y. Y. Schechner, S. G. Narasimhan, and S. K. Nayar, "Polarization-based vision through haze," *Appl. Opt.*, vol. 42, pp. 511–525, 2003, doi: 10.1364/AO.42.000511.

[13] Y. Y. Schechner and N. Karpel, "Recovery of underwater visibility and structure by polarization analysis," *IEEE J. Ocean. Eng.*, vol. 30, no. 3, pp. 570–587, Jul. 2005, doi: 10.1109/JOE.2005.850871.

[14] R. Foster et al., "Retrieval of the polarized submarine light field from above surface measurements using polarimetric imaging," in *Proc. SPIE Commercial + Sci. Sens. Imag.*, 2016, pp. 175–188.

[15] J. Guan, M. Ma, and P. Sun, "Optimization of rotating orthogonal polarization imaging in turbid media via the Mueller matrix," *Opt. Laser Eng.*, vol. 121, pp. 104–111, 2019, doi: 10.1016/j.optlaseng.2019.04.001.

[16] F. Liu et al., "Deeply seeing through highly turbid water by active polarization imaging," *Opt. Lett.*, vol. 43, pp. 4903–4906, 2018, doi: 10.1364/OL.43.004903.

[17] Y. Wei, P. Han, F. Liu, and X. Shao, "Enhancement of underwater vision by fully exploiting the polarization information from Stokes vector," *Opt. Exp.*, vol. 29, no. 14, pp. 22275–22287, 2021, doi: 10.1364/OE.433072.

[18] H. Hu, L. Zhao, X. Li, H. Wang, and T. Liu, "Underwater image recovery under the nonuniform optical field based on polarimetric imaging," *IEEE Photon. J.*, vol. 10, no. 1, Feb. 2018, Art no. 6900309, doi: 10.1109/JPHOT.2018.2791517.

[19] T. Treibitz and Y. Y. Schechner, "Active polarization descattering," *IEEE Trans. Pattern Anal. Mach. Intell.*, vol. 31, no. 3, pp. 385–399, Mar. 2009, doi: 10.1109/TPAMI.2008.85.

[20] J. Liang et al., "Reconfigurable snapshot polarimetric imaging technique through spectral-polarization filtering," *Opt. Lett.*, vol. 44, pp. 4574–4577, 2019, doi: 10.1364/OL.44.004574.

[21] P. Han, F. Liu, Y. Wei, and X. Shao, "Optical correlation assists to enhance underwater polarization imaging performance," *Opt. Laser Eng.*, vol. 134, 2020, Art. no. 106256, doi: 10.1016/j.optlaseng.2020.106256.

[22] S. Y. Lu and R. A. Chipman, "Interpretation of Mueller matrix based on polar decomposition," *J. Opt. Soc. Amer. A.*, vol. 13, pp. 1106–1113, 1996, doi: 10.1364/JOSAA.13.001106.

[23] J. S. Jaffe, "Computer modeling and the design of optimal underwater imaging systems," *IEEE J. Ocean. Eng.*, vol. 15, no. 2, pp. 101–111, Apr. 1990, doi: 10.1109/48.50695.

[24] F. Liu et al., "Depolarization index from Mueller matrix descatters imaging in turbid water," *Chin. Opt. Lett.*, vol. 20, Feb. 2022, Art. no. 022601, doi: 10.3788/COL202220.022601.

[25] Y. I. Moon, B. Rajagopalan, and U. Lall, "Estimation of mutual information using kernel density estimators," *Phys. Rev. E: Statist. Phys., Plasmas, Fluids, Related Interdiscipl. Topics*, vol. 52, pp. 2318–2321, 1995, doi: 10.1103/PhysRevE.52.2318.

[26] Y. Wang, J. Li, Y. Lu, Y. Fu, and Q. Jiang, "Image quality evaluation based on image weighted separating block peak signal to noise ratio," in *Proc. Int. Conf. Neural Netw. Signal Process. IEEE*, 2003, vol. 2, pp. 994–997.

[27] Z. Wang, A. C. Bovik, H. R. Sheikh, and E. P. Simoncelli, "Image quality assessment: From error visibility to structural similarity," *IEEE Trans. Image Process.*, vol. 13, no. 4, pp. 600–612, Apr. 2004, doi: 10.1109/TIP.2003.819861.

[28] M. P. Rowe, E. N. Pugh, J. S. Tyo, and N. Engheta, "Polarization-difference imaging: A biologically inspired technique for observation through scattering media," *Opt. Lett.*, vol. 20, pp. 608–610, 1995, doi: 10.1364/OL.20.000608.